Available online at www.sciencedirect.com
ScienceDirect
Journal of Solid State Chemistry 180 (2007) 1809–1815
JOURNAL OF SOLID STATE CHEMISTRY
www.elsevier.com/locate/jssc

# Synthesis, crystal structure and thermoelectric properties of a new carbide $Zr_2[Al_{3.56}Si_{0.44}]C_5$

Koichiro Fukuda[a,*], Miyuki Hisamura[a], Tomoyuki Iwata[a], Nobuyuki Tera[a], Kimiyasu Sato[b]

[a]*Department of Environmental and Materials Engineering, Nagoya Institute of Technology, Nagoya 466-8555, Japan*
[b]*National Institute of Advanced Industrial Science and Technology (AIST), Nagoya 463-8560, Japan*

Received 15 January 2007; received in revised form 29 March 2007; accepted 1 April 2007
Available online 11 April 2007

**Abstract**

A new quaternary layered carbide, $Zr_2[Al_{3.56}Si_{0.44}]C_5$, has been synthesized and characterized by X-ray powder diffraction, transmission electron microscopy and thermopower and electrical conductivity measurements. The crystal structure was successfully determined using direct methods, and further refined by the Rietveld method. The crystal is trigonal (space group $R3m$, $Z = 3$) with lattice dimensions of $a = 0.331059(5)$, $c = 4.09450(5)$ nm and $V = 0.38864(1)$ nm$^3$. The final reliability indices calculated from the Rietveld refinement were $R_{wp} = 6.24\%$, $R_p = 4.21\%$ and $R_B = 0.82\%$. The crystal structure is composed of electroconductive NaCl-type ZrC slabs separated by $Al_4C_3$-type $[Al_{3.56}Si_{0.44}]C_3$ layers. This material had thermoelectric properties superior to those of the ternary layered carbides $Zr_2Al_3C_4$ and $Zr_3Al_3C_5$, with the power factor reaching $7.6 \times 10^{-5}$ W m$^{-1}$ K$^{-2}$.


*Keywords:* Crystal structure; X-ray diffraction; Rietveld method; Carbides; Thermoelectric properties

## 1. Introduction

Ternary carbides have been extensively studied because of their importance in electrical, mechanical and thermal applications [1,2]. In the Zr–Al–C system, the existence of two compounds, $Zr_2Al_3C_4$ and $Zr_3Al_3C_5$, has been reported [2–4]. Each crystal, belonging to the space group $P6_3mc$, shows intergrowth structure consisting of two types of layers; one is composed of the NaCl-type ZrC and the other consists of $Al_3C_2$ in an atom arrangement very similar to that of $Al_4C_3$ (space group $R\bar{3}m$ [5]). The $Al_3C_2$ layers are the same between the two compounds, while the ZrC slabs are thicker for $Zr_3Al_3C_5$. These two types of layers shear the carbon-atom network at their boundaries; the C–C distances are about 0.335 nm for both compounds. On the other hand, the C–C distance of ZrC crystal is 0.330 nm ($= a(\mathrm{ZrC})/\sqrt{2}$) and that of $Al_4C_3$ is 0.334 nm ($= a(Al_4C_3)$), where $a$(ZrC) and $a(Al_4C_3)$ represent the $a$-axis lengths of the ZrC and $Al_4C_3$ crystals, respectively. These distances are close to each other, and also to those of the carbon-atom networks in $Zr_2Al_3C_4$ and $Zr_3Al_3C_5$. Fukuda et al. have therefore concluded that the closeness of the C–C distances between the ZrC and $Al_4C_3$ crystals, being expressed by the equation $a(\mathrm{ZrC})/\sqrt{2} \sim a(Al_4C_3)$, is the principal reason for the formation of these layered carbides [4].

Thermoelectric materials with high efficiency of energy conversion are of interest for applications as heat pumps and power generators. Low-dimensional materials that consist of, for example, conducting two-dimensional (2D) layers are promising for thermoelectric energy conversion [6–11]. The advantage of the low dimensionality can be interpreted in terms of the carrier confinement effect in the 2D layers, which leads to an enlarged absolute value of the Seebeck coefficient ($S$) compared to the materials with three-dimensional conducting paths. In addition, the 2D layered materials are expected to have relatively low thermal conductivity ($\kappa$) due to phonon scattering at layer interfaces. Hence, materials with layered nanostructures could show high performance of thermoelectricity, which is quantified by a figure of merit $S^2\sigma/\kappa$, where $\sigma$ is electrical conductivity.

*Corresponding author. Fax: +81 52 735 5289.
*E-mail address:* fukuda.koichiro@nitech.ac.jp (K. Fukuda).

0022-4596/$ - see front matter © 2007 Elsevier Inc. All rights reserved.
doi:10.1016/j.jssc.2007.04.004

In the ternary system Al–Si–C, Kidwell et al. [12] have successfully prepared a new carbide $Al_8SiC_7$ and characterized it using an X-ray powder diffraction (XPRD) method. The crystal is hexagonal with $a = 0.33127(7)$ nm and $c = 1.9242(4)$ nm. Because the $a$-axis length is almost equal to $a(ZrC)/\sqrt{2}$, the authors have expected the formation of new quaternary carbides for the reaction products between ZrC and $Al_8SiC_7$.

In the present study, we have prepared a new quaternary carbide in the Zr–Al–Si–C system to determine the crystal structure from XRPD data using direct methods. The crystal structure of the new carbide has been described in relation to those of $Zr_2Al_3C_4$ and $Zr_3Al_3C_5$. Because these carbides are characterized by an intergrowth structure with electroconductive NaCl-type ZrC slabs separated by $Al_4C_3$-type layers, they were expected to show good thermoelectric properties.

## 2. Experimental

### 2.1. Synthesis of a new carbide

The new quaternary carbide was initially recognized as unidentifiable diffraction lines in the XRPD patterns of the reacted ZrC–$Al_8SiC_7$ mixtures. A number of syntheses with a variety of Zr:$Al_8Si$:C ratios were attempted to determine the stoichiometry. The single-phase material was ultimately prepared by the following procedures.

The reagent-grade chemicals of zirconium carbide (KCL Co., Ltd., 99.9%), aluminum (KCL, 99.9%), silicon carbide (KCL, 99.9%) and graphite (KCL, 99.9%) were mixed in molar ratios of ZrC:Al:SiC:C = 18:32:4:23, which is equivalent to

$$Zr : Al : Si : C = 18 : 32 : 4 : 45. \quad (1)$$

The mixture was pressed into compacts (10 mm × 10 mm × 5 mm), loaded into a graphite crucible, and then embedded in $Al_4C_3$ powder, which was in advance prepared from the chemicals of aluminum and graphite. They were heated in vacuum at 1973 K for 1 h, followed by cooling to ambient temperature by cutting furnace power. The $Al_4C_3$ powder was allowed to gradually evaporate during heating, keeping the stoichiometry of the compact samples unchanged. The reaction product was a slightly sintered polycrystalline material. It was finely ground to obtain powder specimen. The density ($D_o$) of the powder specimen was subsequently measured by the pyknometric method and found to be 4.50 Mg m$^{-3}$.

In order to obtain a dense sample, the powder specimen was subsequently sintered by a pulse electric current sintering method (SPS-1030, Sumitomo Coal Mining). The sintering was conducted at a uniaxial pressure of about 40 MPa and at 1973 K for 5 min in vacuum. Dense sintered bodies in the form of discs (15 mm diameter and 5 mm long) were thus obtained. Its closed porosity was found to be about 99%.

### 2.2. Synthesis of $Zr_2Al_3C_4$ and $Zr_3Al_3C_5$

Two types of sintered specimens of $Zr_2Al_3C_4$ and $Zr_3Al_3C_5$ were individually prepared from the reagent-grade chemicals of zirconium carbide, aluminum and graphite. Each of the stoichiometric mixtures was first heated in vacuum at 1653 K for 1 h to obtain polycrystalline materials. The sintering conditions to prepare the dense bodies were identical to those described above. Their closed porosities were found to be about 99% for both samples.

### 2.3. Structural characterization

The XRPD intensities for structural determination were collected for the powder specimen on a PANalytical X'Pert diffractometer in Bragg–Brentano geometry using monochromatized Cu$K\alpha$ radiation (50 kV, 40 mA) and a step-scan technique in a $2\theta$ range from 10° to 149.98° with a fixed counting time ($t$) of 15 s/step and a step interval of 0.02°. The divergence slit of 1° was employed to collect the quantitative profile intensities in the range $2\theta \geqslant 19°$. The crystal-structure models were visualized with the computer program VICS [13]. The structure data were standardized using the computer program STRUCTURE TIDY [14].

The powder specimen was also examined using a transmission electron microscope (TEM:JEM 2010, JEOL) operated at 200 kV. The crystal fragments were crushed using an agate mortar and deposited with ethyl alcohol on a copper grid. A selected area electron diffraction (SAED) pattern and corresponding lattice image were obtained.

### 2.4. Thermoelectric properties

Samples in the form of rectangular bars (13 mm × 4 mm × 3 mm) were cut from the discs using a diamond saw for thermoelectric measurements. The X-ray diffraction intensities from the cut surface have revealed that the sintered samples, consisting exclusively of the desired phases, were free from preferred orientation of the crystal grains. The thermoelectric properties were evaluated by the power factor, which is determined from electrical conductivity ($\sigma$) and Seebeck coefficient ($S$) as $S^2\sigma$. The $\sigma$-values and thermoelectromotive force (TF) were simultaneously measured between 373 and 1273 K in vacuum using a thermoelectric property measurement system (RZ2001i, Ozawa Science). It generated a temperature gradient in the specimen by passing cool air in a silica glass tube that is placed near one end of the specimen. The TF-values were measured as a function of temperature difference ($\Delta T$) between the two ends. The $S$-values were calculated from the slopes of the linear plots of TF against $\Delta T$.

## 3. Results and discussion

### 3.1. Chemical formula and Z

The SAED pattern in Fig. 1(a) was successfully indexed with a hexagonal unit cell with dimensions of $a \approx 0.33$ nm and $c \approx 4.1$ nm. The corresponding lattice image (Fig. 1(b)) strongly suggests that the crystal structure is built up from stacking combinations of two basic sheets. The unit-cell parameters as well as integrated intensities were refined by the whole powder-pattern decomposition method, based on the Pawley algorithm [15], using the computer program WPPF [16] in the $2\theta$ range from 10° to 70°. The refined unit-cell parameters are $a = 0.330821(7)$ nm, $c = 4.0914(1)$ nm and $V = 0.38778(2)$ nm$^3$. The refined integrated intensities were examined to confirm the presence or absence of reflections. There were systematic absences $h-k+l \neq 3n$ for $h\,k\,i\,l$, $-h+l \neq 3n$ for $h\,h\,0\,l$, $l \neq 3n$ for $h\,h\,2\,h\,l$ and $l \neq 3n$ for $0\,0\,0\,l$, implying that the possible space groups are $R3$, $R\bar{3}$, $R32$, $R3m$ and $R\bar{3}m$.

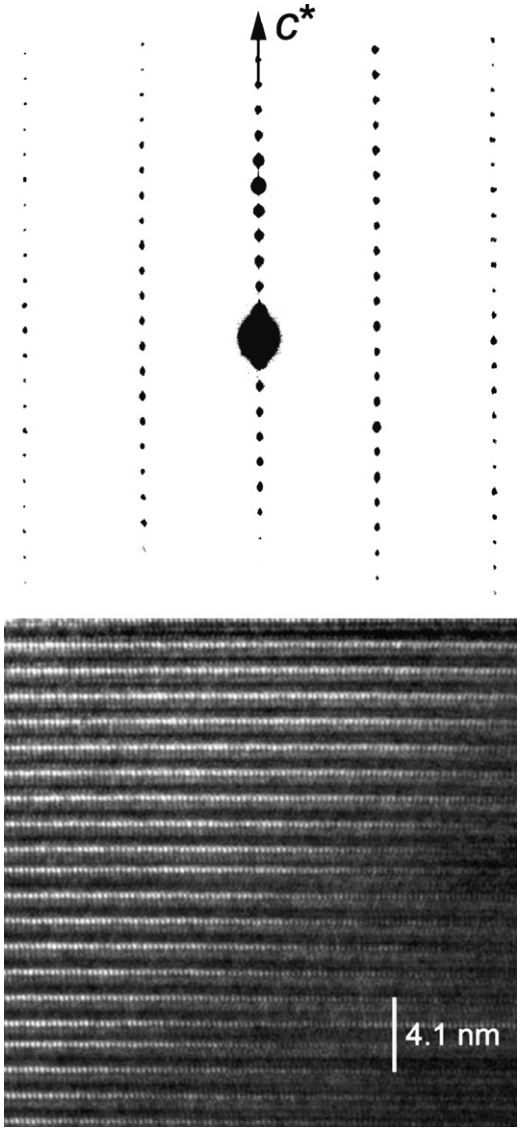


Fig. 1. (a) Selected-area electron diffraction pattern and (b) corresponding lattice image. Incident beam perpendicular to the $c$-axis.

In general, the number of formula units in the unit cell ($Z$) is determined from the unit-cell volume $V$ (nm$^3$), true density $D_t$ (Mg m$^{-3}$) and molecular weight $M$ (g) as follows [17]:

$$Z = VD_t/(M \times 1.660 \times 10^{-3}). \quad (2)$$

Substituting 0.38778 nm$^3$ and 4.50 Mg m$^{-3}$ ($= D_o$) for, respectively, $V$-value and $D_t$-value in Eq. (2) yields the following equation:

$$Z \approx 1052/M. \quad (3)$$

The $Z$-value is integer and is also subject to space group restrictions. Because the smallest value for *number of positions* of each possible space group is three, the smallest integral value for $Z$ allowed by all the space groups is three. When we set $Z = 3$, Eq. (3) becomes

$$M \approx 350.7. \quad (4)$$

Accordingly, the chemical formula which satisfies both Eqs. (1) and (4) is $Zr_2[Al_{3.56}Si_{0.44}]_{\sum 4}C_5$ ($M = 350.92$).

### 3.2. Crystal structure determination

All of the possible space groups were tested using the EXPO2004 package [18] for crystal structure determination. Because the atomic scattering factors for Al and Si are almost the same, a unit cell content with [6Zr 12Al 15C] was used as input data for the search of a crystal-structure model. A promising structural model with the reliability index $R_F$ [19] of 14.3% was successfully obtained for the space group $R3m$.

Structural parameters were refined by the Rietveld method using the computer program RIETAN-2000 [20] in the $2\theta$ range of 22.0–149.0° (Fig. 2). The Si and Al atoms were assumed to be randomly distributed over the same sites (denoted by $T$) in the crystal structure, although there might be the site preference of these atoms. A Legendre polynomial was fitted to background intensities with 12 adjustable parameters. The pseudo-Voigt function [21] was used to fit the peak profile. All of the isotropic atomic displacement parameters ($B$) of carbon atoms were constrained to have the same value. Reliability indices for a final result were $R_{wp} = 6.24\%$, $R_p = 4.21\%$ and $R_B = 0.82\%$ [19]. Crystal data are given in Table 1, and the final atomic positional and $B$ parameters are given in Table 2. The selected interatomic distances, together with their standard deviations, are given in Table 3.

### 3.3. Structure description

The crystal structure of $Zr_2[Al_{3.56}Si_{0.44}]C_5$ may be regarded as intergrowth structure, which consists of the NaCl-type ZrC layers with thickness of about 0.57 nm separated by the $(Al_{3.56}Si_{0.44})C_3$ layers (about 0.80 nm thickness) in an atom arrangement very similar to that of

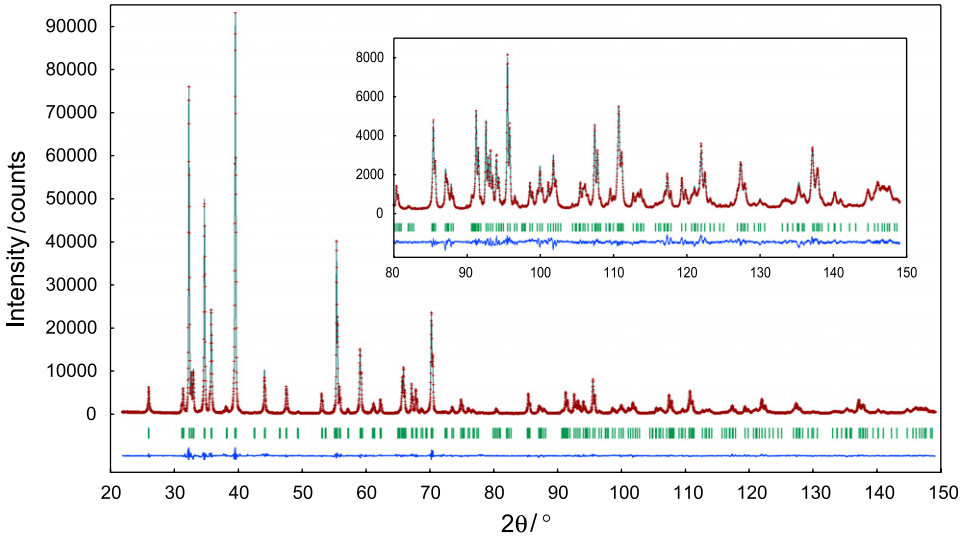


Fig. 2. Comparison between observed (+ marks) and calculated (upper solid line) patterns of $Zr_2[Al_{3.56}Si_{0.44}]C_5$. The difference curve is shown in the lower part of the figure. Vertical marks indicate the positions of possible Bragg reflections.

Table 1
Crystal data for $Zr_2[Al_{3.56}Si_{0.44}]C_5$

| | |
|---|---|
| Chemical composition | $Zr_2[Al_{3.56}Si_{0.44}]C_5$ |
| Space group | *R*3*m* |
| *a* (nm) | 0.331059(5) |
| *c* (nm) | 4.09450(5) |
| *V* ($nm^3$) | 0.38864(1) |
| *Z* | 3 |
| *Dx* ($Mg\,m^{-3}$) | 4.50 |

Table 2
Structural parameters for $Zr_2[Al_{3.56}Si_{0.44}]C_5$[a]

| Atom | *x* | *y* | *z* | $100 \times B$ ($nm^2$) |
|---|---|---|---|---|
| Zr1 | 0 | 0 | 0.6267(3) | 0.18(6) |
| Zr2 | 0 | 0 | 0.8952(3) | 0.19(6) |
| *T*1 | 0 | 0 | 0.0693(3) | 0.8(1) |
| *T*2 | 0 | 0 | 0.1732(4) | 0.5(2) |
| *T*3 | 0 | 0 | 0.3504(4) | 0.4(2) |
| *T*4 | 0 | 0 | 0.4494(2) | 0.7(1) |
| C1[b] | 0 | 0 | 0 | 0.20(6) |
| C2 | 0 | 0 | 0.1279(3) | 0.20 |
| C3 | 0 | 0 | 0.2635(5) | 0.20 |
| C4 | 0 | 0 | 0.4006(3) | 0.20 |
| C5 | 0 | 0 | 0.5289(2) | 0.20 |

[a]All atoms are in Wyckoff position 3*a*.
[b]*z* of C1 atom is fixed.

Table 3
Interatomic distances (nm) in $Zr_2[Al_{3.56}Si_{0.44}]C_5$[a]

| | | | |
|---|---|---|---|
| Zr1–C3 | 0.2269(9) × 3 | *T*4–C2 | 0.1972(3) × 3 |
| Zr1–C1 | 0.2517(7) × 3 | *T*4–C4 | 0.1997(11) |
| Zr1–*T*3 | 0.3017(7) × 3 | *T*4–*T*1 | 0.2705(3) × 3 |
| Zr1–Zr2 | 0.32719(8) × 3 | *T*4–*T*2 | 0.3019(11) × 3 |
| Zr1–Zr1 | 0.33106(1) × 6 | *T*4–C5 | 0.3254(12) |
| Zr2–C5 | 0.2339(6) × 3 | *T*4–*T*4 | 0.33106(1) × 6 |
| Zr2–C3 | 0.2389(10) × 3 | C1–*T*3 | 0.2035(6) × 3 |
| Zr2–*T*2 | 0.2964(7) × 3 | C1–Zr1 | 0.2517(7) × 3 |
| Zr2–Zr1 | 0.32719(8) × 3 | C1–*T*1 | 0.2839(12) |
| Zr2–Zr2 | 0.33106(1) × 6 | C2–*T*2 | 0.1852(15) |
| *T*1–C4 | 0.19132(5) × 3 | C2–*T*4 | 0.1972(3) × 3 |
| *T*1–C2 | 0.2400(14) | C2–*T*1 | 0.2400(14) |
| *T*1–*T*4 | 0.2705(3) × 3 | C3–Zr1 | 0.2269(9) × 3 |
| *T*1–C1 | 0.2839(12) | C3–Zr2 | 0.2389(10) × 3 |
| *T*1–*T*3 | 0.2871(10) × 3 | C4–*T*1 | 0.19132(5) × 3 |
| *T*1–*T*1 | 0.33106(1) × 6 | C4–*T*4 | 0.1997(11) |
| *T*2–C2 | 0.1852(15) | C4–*T*3 | 0.2058(14) |
| *T*2–C5 | 0.2120(7) × 3 | C5–*T*2 | 0.2120(7) × 3 |
| *T*2–Zr2 | 0.2964(7) × 3 | C5–Zr2 | 0.2339(6) × 3 |
| *T*2–*T*4 | 0.3019(11) × 3 | C5–*T*4 | 0.3254(12) |
| *T*2–*T*2 | 0.33106(1) × 6 | | |
| *T*3–C1 | 0.2035(6) × 3 | | |
| *T*3–C4 | 0.2058(14) | | |
| *T*3–*T*1 | 0.2871(10) × 3 | | |
| *T*3–Zr1 | 0.3017(7) × 3 | | |
| *T*3–*T*3 | 0.33106(1) × 6 | | |

[a]All distances shorter than 0.34 nm (metal–metal) and 0.33 nm (metal–carbon) are given.

$Al_4C_3$ (Fig. 3). These two types of layers shear the two-dimensional networks of carbon atoms at their boundaries with the C–C distance of 0.3311 nm. The lattice image in Fig. 1(b) is fully consistent with the layered structure.

The mean interatomic distances in $Zr_2[Al_{3.56}Si_{0.44}]C_5$ compare well with those of the binary and ternary carbides (i.e., ZrC, $Al_4C_3$, $Zr_2Al_3C_4$ and $Zr_3Al_3C_5$). Both Zr1 and Zr2 atoms are octahedrally coordinated by C atoms with the mean Zr–C distance of 0.238 nm (Table 3), which is comparable to those of the $ZrC_8$ polyhedra in ZrC (0.235 nm), $Zr_2Al_3C_4$ (0.241 nm) [4] and $Zr_3Al_3C_5$ (0.239 nm) [3]. The Zr atoms have 12 metal neighbors as in $Zr_2Al_3C_4$ and $Zr_3Al_3C_5$. The mean Zr–Zr distance of 0.329 nm in $Zr_2[Al_{3.56}Si_{0.44}]C_5$ is comparable to those of ZrC (0.332 nm), $Zr_2Al_3C_4$ (0.335 nm) and $Zr_3Al_3C_5$ (0.331 nm).

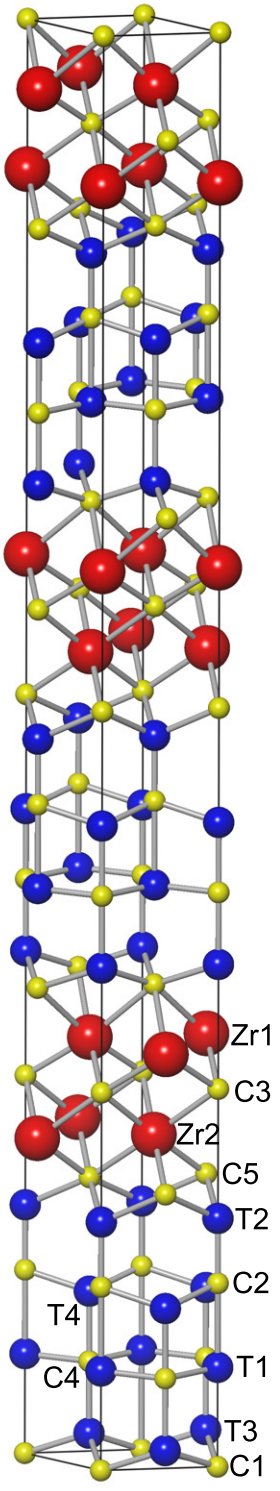


Fig. 3. Crystal structure of $Zr_2[Al_{3.56}Si_{0.44}]C_5$.

The Al and/or Si atoms on $T$ sites are tetrahedrally coordinated with the mean distances of 0.220 nm for $T1$–C, 0.205 nm for $T2$–C, 0.204 nm for $T3$–C and 0.223 nm for $T4$–C. Accordingly, the $T$–C distances are comparable to the Al–C distances of the $AlC_4$ tetrahedra in $Al_4C_3$,

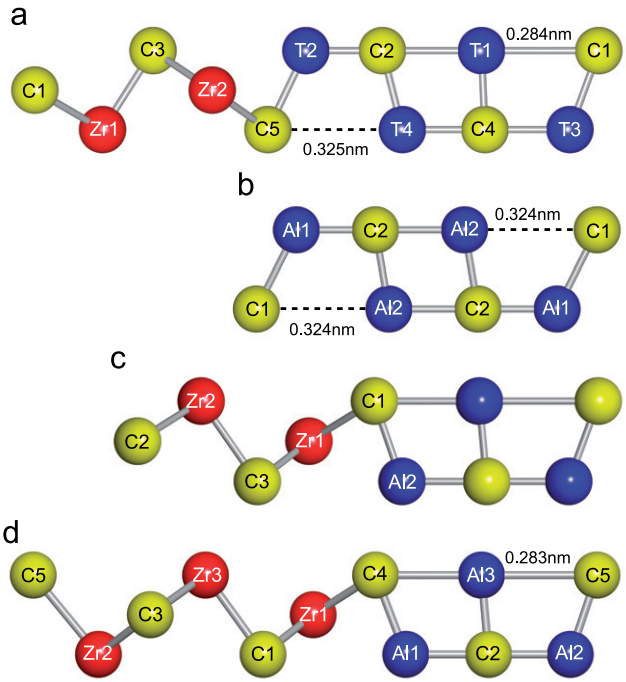


Fig. 4. Atomic configurations in (a) $Zr_2[Al_{3.56}Si_{0.44}]C_5$, (b) $Al_4C_3$, (c) $Zr_2Al_3C_4$, and (d) $Zr_3Al_3C_5$. The atom numbering in (b)–(d) follows that of the original manuscripts [3–5].

ranging from 0.194 to 0.218 nm (the mean = 0.206 nm) [5]. The mean Zr–$T$ distance of 0.299 nm in $Zr_2[Al_{3.56}Si_{0.44}]C_5$ is comparable to the Zr–Al distances of $Zr_2Al_3C_4$ (0.297 nm) [4], $Zr_3Al_3C_5$ (0.297 nm) [3] and $Al_3Zr$ (0.291 nm) [22].

In Fig. 4, the atomic configurations and selected interatomic distances are shown for $Zr_2[Al_{3.56}Si_{0.44}]C_5$, $Al_4C_3$ [5], $Zr_2Al_3C_4$ [4] and $Zr_3Al_3C_5$ [3]. The Al and/or Si atoms in $Zr_2[Al_{3.56}Si_{0.44}]C_5$ are tetrahedrally coordinated as in $Al_4C_3$. Moreover, the distances of about 0.325 nm for $T4$–C5 [Fig. 4(a)] is close to the corresponding distance of Al2–C1 (0.324 nm) in $Al_4C_3$ [Fig. 4(b)]. Accordingly, the $(Al_{3.56}Si_{0.44})C_3$ layer in $Zr_2[Al_{3.56}Si_{0.44}]C_5$ is structurally comparable to the compound $Al_4C_3$. On the other hand, the coordination number of Al3 in $Zr_3Al_3C_5$ [Fig. 4(d)] is five if C5 atoms at relatively long distance of 0.283 nm are included into the $[AlC_5]$ unit. The Al3 atoms are therefore located in trigonal bipyramidal voids formed by five carbon atoms. This is one of the prominent features of the $Zr_3Al_3C_5$ structure as pointed out by Gesing and Jeitschko [3]. The situation is nearly the same for Al1 and C2 atoms in $Zr_2Al_3C_4$ [Fig. 4(c)].

### 3.4. Thermoelectric properties

The $\sigma$-values of the three samples steadily decreased with increasing temperature, representing a conductor-type behavior (Fig. 5(a)). When samples were compared at the same temperature, $Zr_3Al_3C_5$ always showed the largest $\sigma$-value, followed by $Zr_2[Al_{3.56}Si_{0.44}]C_5$. Because the $\sigma$-value

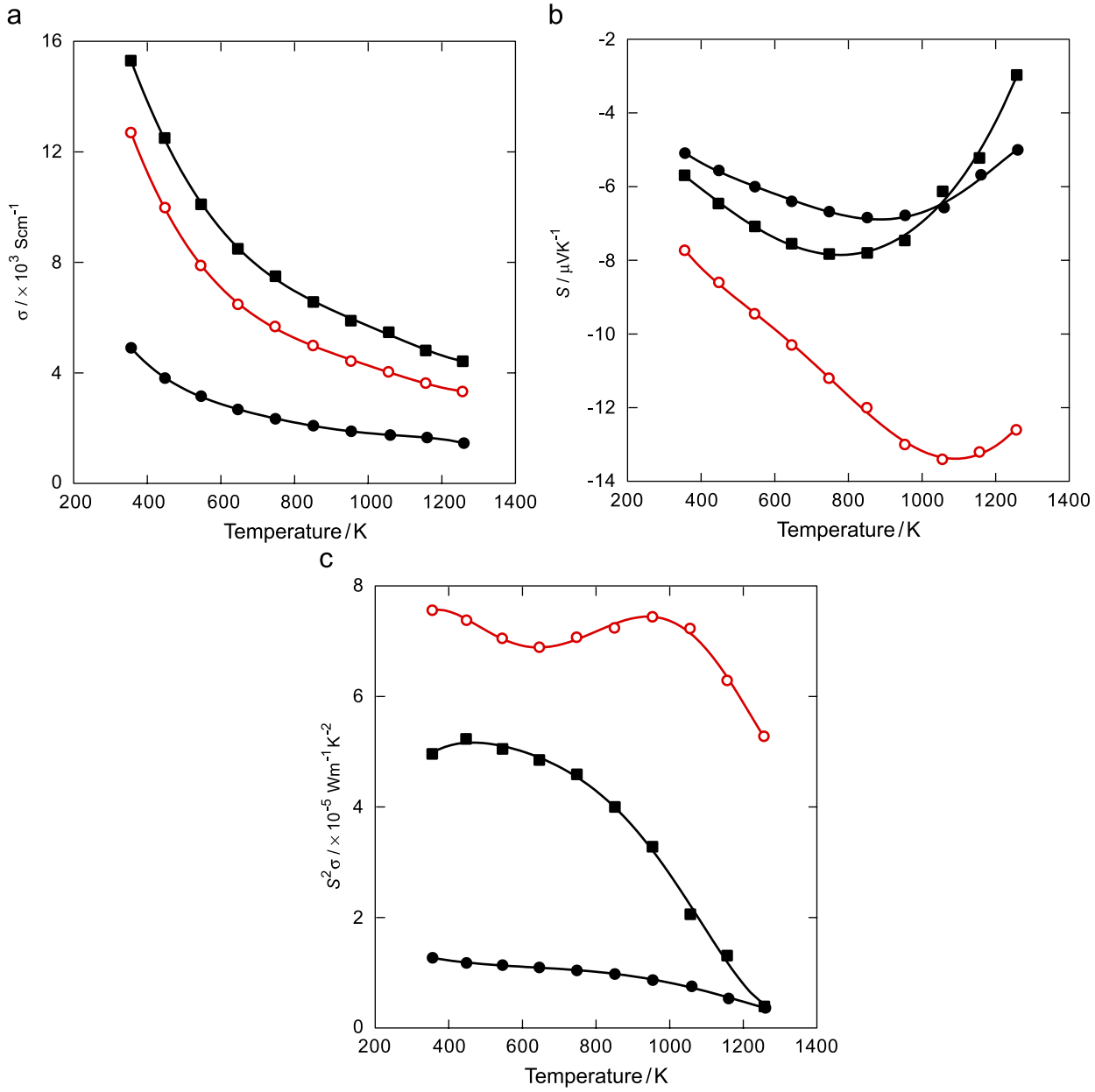


Fig. 5. Temperature dependence of (a) electrical conductivity $\sigma$, (b) Seebeck coefficient $S$ and (c) thermoelectric power factor $S^2\sigma$ for (open circle) $Zr_2[Al_{3.56}Si_{0.44}]C_5$, (solid circle) $Zr_2Al_3C_4$ and (solid square) $Zr_3Al_3C_5$.

of $Zr_3Al_3C_5$ was much larger than that of $Zr_2Al_3C_4$, the intergrowth structure with thicker ZrC layer appears to be more advantageous for the conduction of electricity.

The signs of $S$ were always negative for all the samples, indicating predominant negative mobile charge carriers (Fig. 5(b)). With $Zr_2[Al_{3.56}Si_{0.44}]C_5$, the absolute value of $S$ was the largest among the three, throughout the temperature region measured, and steadily increased with increasing temperature from 373 to 1073 K. A comparison of the $S$-values between $Zr_2[Al_{3.56}Si_{0.44}]C_5$ and $Zr_2Al_3C_4$ suggests that the intergrowth structure with the thicker $Al_4C_3$-type layer would be more favorable for the thermoelectric power generation.

The power-factor values for $Zr_2Al_3C_4$ and $Zr_3Al_3C_5$ decreased from, respectively, $1.3\times10^{-5}$ and $5.2\times10^{-5}\,W\,m^{-1}\,K^{-2}$ with increasing temperature. On the other hand, the power-factor values of $Zr_2[Al_{3.56}Si_{0.44}]C_5$ was almost constant between 373 and 1073 K and necessarily the largest among the three, with the maximal value of $7.6\times10^{-5}\,W\,m^{-1}\,K^{-2}$ at 373 K (Fig. 5(c)). Since all the present sintered specimens were composed of randomly oriented polycrystals, the improvement of preferred orientation using the technique of ceramic processing or thin film preparation could further increase the electrical conductivity and consequently the power factor.

## Acknowledgments

Supported by a Grant-in-Aid for Scientific Research (no. 18560654) from the Japan Society for the Promotion of Science, and a grant from the Thermal and Electric Energy Technology Foundation in Japan.

## References

[1] U. Ruschewitz, Coord. Chem. Rev. 244 (2003) 115–136.
[2] J.C. Schuster, H. Nowotny, Z. Metallkde. 71 (1980) 341–346.
[3] Th.M. Gesing, W. Jeitschko, J. Solid State Chem. 140 (1998) 396–401.
[4] K. Fukuda, S. Mori, S. Hashimoto, J. Am. Ceram. Soc. 88 (2005) 3528–3530.
[5] Th.M. Gesing, W. Jeitschko, Z. Naturforsch. 50b (1995) 196–200.
[6] L.D. Hicks, M.S. Dresselhaus, Phys. Rev. B 47 (1993) 12727–12731.
[7] L.D. Hicks, M.S. Dresselhaus, Phys. Rev. B 47 (1993) 16631–16634.
[8] L.D. Hicks, T.C. Harman, M.S. Dresselhaus, Appl. Phys. Lett. 63 (1993) 3230–3232.
[9] K. Koumoto, H. Koduka, W.-S. Seo, J. Mater. Chem. 11 (2001) 251–252.
[10] M. Yasukawa, K. Ikeuchi, T. Kono, K. Ueda, H. Hosono, J. Appl. Phys. 98 (2005) 013706/1–013706/4.
[11] T. Mori, T. Nishimura, J. Solid State Chem. 179 (2006) 2908–2915.
[12] B.L. Kidwell, L.L. Oden, R.A. McCune, J. Appl. Crystallogr. 17 (1984) 481–482.
[13] F. Izumi, R.A. Dilanian, IUCr Newslett. 32 (2005) 59–63.
[14] L.M. Gelato, E. Parthé, J. Appl. Crystallogr. 20 (1987) 139–143.
[15] G.S. Pawley, J. Appl. Crystallogr. 14 (1981) 357–361.
[16] H. Toraya, J. Appl. Crystallogr. 19 (1986) 440–447.
[17] J.W. Jeffery, Methods in X-ray Crystallography, Academic Press, London, UK, 1971.
[18] A. Altomare, M.C. Burla, M. Camalli, B. Carrozzini, G.L. Cascarano, C. Giacovazzo, A. Guagliardi, A.G.G. Moliterni, G. Polidori, R. Rizzi, J. Appl. Crystallogr. 32 (1999) 339–340.
[19] R.A. Young (Ed.), The Rietveld Method, Oxford University Press, Oxford, UK, 1993, pp. 1–38.
[20] F. Izumi, in: R.A. Young (Ed.), The Rietveld Method, Oxford University Press, Oxford, UK, 1993, pp. 236–253.
[21] H. Toraya, J. Appl. Crystallogr. 23 (1990) 485–491.
[22] Y. Ma, C. Romming, B. Lebech, J. Gjonnes, J. Tafto, Acta Crystallogr. B 48 (1992) 11–16.